Missouri University of Science and Technology
Scholars' Mine

Materials Science and Engineering Faculty Research & Creative Works

Materials Science and Engineering

01 Jan 2023

Phenomenological Analysis Of Surface Degradation Of Metallic Materials In Extreme Environment

Simon N. Lekakh
Missouri Unviersity of Science and Technology, lekakhs@mst.edu

Oleg Neroslavsky

Follow this and additional works at: https://scholarsmine.mst.edu/matsci_eng_facwork

 Part of the Metallurgy Commons

Recommended Citation

S. N. Lekakh and O. Neroslavsky, "Phenomenological Analysis Of Surface Degradation Of Metallic Materials In Extreme Environment," *Metallurgical and Materials Transactions A: Physical Metallurgy and Materials Science*, Springer; ASM International, Jan 2023.
The definitive version is available at https://doi.org/10.1007/s11661-023-07234-2

This Article - Journal is brought to you for free and open access by Scholars' Mine. It has been accepted for inclusion in Materials Science and Engineering Faculty Research & Creative Works by an authorized administrator of Scholars' Mine. This work is protected by U. S. Copyright Law. Unauthorized use including reproduction for redistribution requires the permission of the copyright holder. For more information, please contact scholarsmine@mst.edu.

ORIGINAL RESEARCH ARTICLE

Phenomenological Analysis of Surface Degradation of Metallic Materials in Extreme Environment

SIMON N. LEKAKH and OLEG NEROSLAVSKY

The resistance to surface degradation in metallic alloys plays an important role for the lifetime of the components working in harsh environments. The mechanisms involved in degradation of metallic surface in a high-temperature aggressive gaseous atmosphere include the following: forming adherent to the surface multiphase oxide layer, partial spallation, and possible vaporization of formed compounds. The governing equation, which describes a parabolic growth of adherent layer, time-dependent vaporization, and cross-linked to instantaneous thickness of adherent layer spallation rate, was suggested and analyzed. The several relationships between the kinetic constants were defined from analysis of the governing equation. Design of routes for experimental procedures to determine the independent kinetic constants was discussed and an integrated simulator was used to calculate the kinetic constants based on experimental results. Two examples of high-temperature oxidation of heat-resistant Cr/Ni austenitic steel were used to illustrate the capability of the suggested method to determine the oxidation, spallation, and vaporization kinetic constants from a single experiment. The suggested methodology could be considered in future for the analysis of different types of surface degradation of solid materials in gaseous, liquid, or solid environments.

https://doi.org/10.1007/s11661-023-07234-2
© The Minerals, Metals & Materials Society and ASM International 2023

I. INTRODUCTION

THE resistance to surface degradation in metallic alloys plays an important role for the lifetime of the components working in harsh environments. There are several distinguishing categories of surface degradation of solid metallic materials which depend on the aggregate state of the interacting environment (solid, liquid, or gaseous). Table I presents a variety of surface degradation processes of solid metallic materials during interaction with working environment having different aggregate states:

- tribological, in the case of forced interaction with a *solid* environment, such as wear and microfracture,
- electro-chemical corrosion and erosion in a *liquid* environment, such as water solutions, molten salt, and liquid metals,
- chemical modification in a high-temperature *gaseous* environment, such as oxidation, followed by fracture and spallation of the oxide layer due to thermo-mechanical stress and possible vaporization into the surrounding gaseous environment or vacuum.

Different hierarchies of multiscale experimental study and simulations, from atomic[13] to microscopic[14] and macroscopic[15] levels, are used for determination of metallic surface degradation in harsh environments with the goals to develop protection methods and improve metallic component performance. Applications of governing laws and equations are important for the analysis of macro-processes of surface degradation and for finding kinetic constants. A historical review of pioneering works in micro-kinetics of high-temperature solid-state diffusion was done in Reference 16. Fick's diffusion laws are used to describe the macroscopic growth of oxide layer on metallic surface. The forming multilayered oxide scale on surface of metallic alloys,[17] grain boundary diffusion,[18] stress between formed oxide layer and the metal matrix,[19,20] thermo-mechanical spallation,[8,21,22] chemical and structural modification of the formed oxide layer in water vapor environment,[23] vaporization of formed compounds,[24] and much more made it difficult to develop the hierarchy of seamless models from atomic to macroscopic levels. Therefore, the empirical models and numerical approaches were used[25–32] to predict the oxidation kinetics of several alloys as a function of time, temperature, cycle duration. and atmosphere. These models described oxidation-induced surface degradation during

SIMON N. LEKAKH is with the Missouri University of Science and Technology, Rolla, MO 65409. Contact e-mail: lekakhs@mst.edu OLEG NEROSLAVSKY is with the West Long Island LLP, Long Island City, NY 11101.
Manuscript submitted August 4, 2023; accepted October 10, 2023.

Published online: 26 October 2023

Table I. Different Surface Degradation Processes Described in Referenced Reviews

Aggregate State of Interacting Environment	Type of Surface Degradation	Typical Temperature Range	Surface Degradation Mechanism
Solid	tribological	from low to medium	wear, microfractures[1]
Liquid (Water, Salt, Melt)	electro-chemical	from room to high	corrosion, erosion[2–5]
Gaseous	thermo-chemical and thermo-mechanical	from medium to high	oxidation, spallation, vaporization[6–12]

high-temperature exposure. However, there is a lack of an universal physics-based approach to predict the rates of different surface degradation processes considering the severity of environmental loading.

The goal of this study is a development of macroscopic formalism of metallic material behavior in extreme gaseous high-temperature environments. A formalism covers the major processes responsible for surface degradation and it is used for planar solid surface geometry, the case when the dimension of surface degradation is significantly less than geometrical surface curvature. It also suits to "infinity" environmental conditions, meaning that surface degradation is not limited or restricted due to environment exhaustion, for example, decreasing oxidant concentration during intensive oxidation. Instead, surface degradation depends on material properties and the specific environmental conditions (temperature, atmosphere, mechanical load), rather than the quantity of environment, including the volume and concentration of gaseous oxidant.

II. ANALYTICAL REPRESENTATION OF SURFACE DEGRADATION OF METALLIC MATERIALS

The degradation processes of solid metallic surfaces have a diversity of mechanisms and driving forces; however, the overall intensity of macro-degradation of the metallic surface in contact with an "infinity" environment (solid, liquid, or gas) could be quantified using the suggested analytical representations. For infinite-environmental conditions, the rate of surface degradation (Ω) could be the result of two categories of interaction processes. The first category is a surface modification which has a time-dependent rate ($\Psi(\tau)$). An example of such a category is the formation of an oxide protection layer during high-temperature oxidation. Processes which belong to the second category relate to destruction of modified surfaces. The surface destruction processes can be as follows: (i) with time-dependent rate ($\Phi(\tau)$), as in the process of the vaporization of formed species within high-temperature gaseous atmosphere; (ii) cross-depended as a function of instant surface condition ($\Theta(X)$), as in process of the oxide layer spallation due to strain, and dependent on instant oxide layer thickness X.

The balance of these processes could be presented in the suggested general form of surface degradation kinetics (Eq. [1]), where the rate of dense adherent oxide layer Ω is expressed through $\Psi(\tau)$, $\Phi(\tau)$, and $\Theta(X)$, which are the rates of oxidation, vaporization, and spallation correspondingly:

$$\Omega = \Psi(\tau) - \Phi(\tau) - \Theta(X) \quad [1]$$

Equation [1] is applicable for different types of surface degradation of solid material interacting with environments having solid, liquid, or gaseous aggregate states (Table I). For example, it could be surface degradation by oxidation in gaseous atmosphere, erosion in aggressive liquids, or wear by solid particles. The main used assumptions used in governing Eq. [1] included:

- planar surface geometry when the dimension of surface degradation is significantly less than geometrical surface curvature;
- process occurred in infinity environment when surface degradation is not limited or restricted due to environment exhaustion;
- two independent surface degradation kinetics, the first one is time dependent, such as vaporization, and the second one is related to instantaneous degraded surface condition, such as spallation with intensity depended on instant thickness of oxidized surface.

The subject of this study is limited by the macro-phenomenal representation of surface degradation of metallic alloys in harsh high-temperature gaseous environments. Depending on the severity of gaseous environmental loading (temperature, atmosphere, pressure), the surface degradation process could be qualified as *normal*, *extreme*, or uncontrolled destruction of the internal body, which could be considered as *catastrophic* and shown by dotted line in Figure 1. Because of the different nature, we did not describe catastrophic failure in this article. The microstructures in Figures 1(c) and (d) provide an illustration of the oxide layer structure on the surface of a heat-resistant austenitic Cr/Ni steel at different gas environment load severity (temperature and atmosphere), which was studied in Reference 33.

At the *normal* load severity condition in an infinitely high-temperature gaseous environment, the rate of development of oxide layer on metallic surface is controlled by element diffusion. In this case, the kinetics of the growing oxide layer with thickness (X) obeys a parabolic law for time (τ) with kinetic constant K_p (Eq. [2]) and the rate Ψ from Eq. [1] is given in Eq. [3][25]:

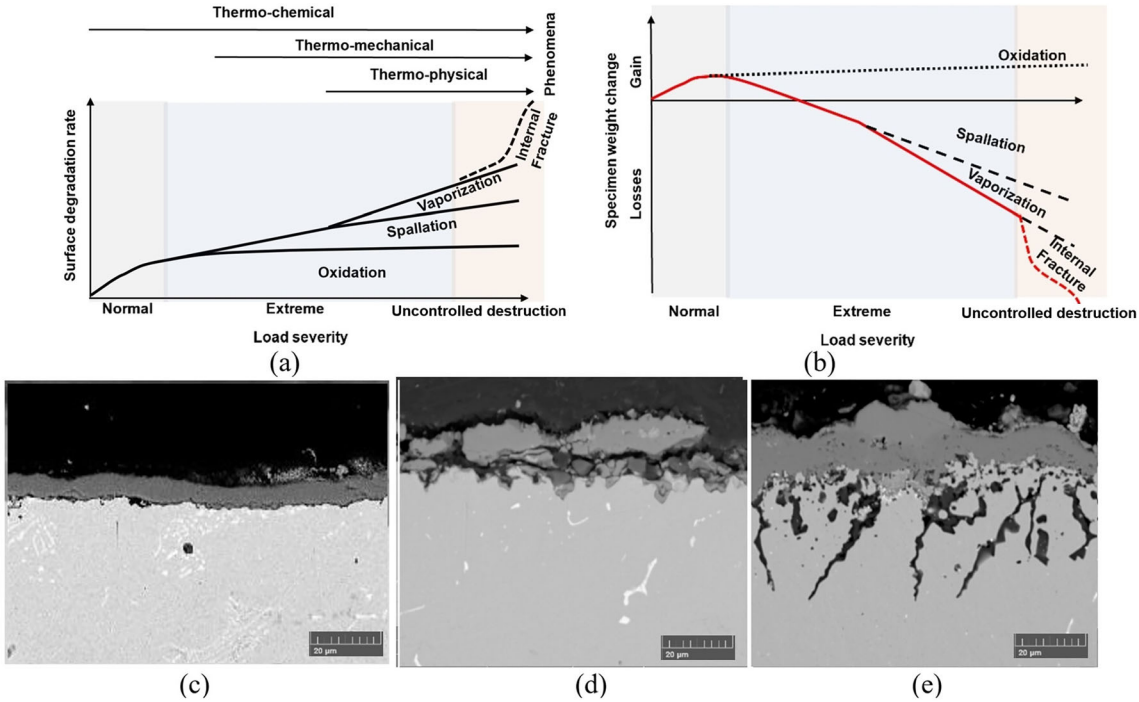

Fig. 1—Schematic illustration of the effect of severity of gaseous environmental loading on involved phenomena of surface degradation (*a*), weight change of specimen due to different surface degradation processes (oxidation, spallation, and vaporization (*b*), and examples of multilayered scale structure in Cr/Ni austenitic steel after 400 h tests using different environmental load severity: normal (*c*), extreme (*d*), and uncontrolled destruction of the internal body (*e*). Steel composition and test parameters are given in Refs. [33,34].

$$X^2 = K_P \tau \qquad [2]$$

$$\Psi = K_P / 2X \qquad [3]$$

In the *normal* load severity of gaseous environment (Figure 1), the specimen gained weight equals to the amount of reacted oxidizer, and it will parabolically decline with increasing oxide thickness X at the rate Ψ. Because the thickness of a surface layer declines with time, such surface modification could be used for protection and thermo-mechanical stability of formed oxide can be predicted with Wagner's theory described in Reference 35. In the multicomponent metallic alloys, a multilayered oxide structure is formed, consisting of the internal and external oxide layers having different phases. Figure 1(c) illustrates a multilayered structure in oxidized Cr/Ni steel, where the external layer consists of iron oxide, and the internal layer includes Cr–Fe–Mn oxides.[33,34] Such complicated processes could have deviations from a parabolic law (Eq. [3]) and kinetic curves observed in experiments were fitted to the models with linear, parabolic, or cubic[36] time dependencies of function Ψ. At the normal environmental load severity (Figure 1(c)), the overall rate of the formed oxide layer $\Psi(\tau)$ declined with a process time for all used models.

Increasing severity of gaseous environment (temperature, gas reactivity, pressure) and thermo-mechanical stress generate different types of imperfections in the oxide layer, such as point type vacancies, micro-voids, and cracks (Figure 1(d)). These imperfections initiate surface degradation processes, such as buckling and spallation of oxide layer.[8] Relaxation of the strain energy will take place *via* plastic or creep deformation of the oxide scale and the alloy or cracking and/or spallation of the scale.[21] Continuation of increasing severity of environmental loading propagates surface degradation into the metal matrix (Figure 1(e)), which could lead to catastrophic failure of metallic components. The increasing severity of gaseous environmental loading moves the surface degradation process from the "normal" type, when formed oxide layer protects component body, to "extreme," when oxide layer delamination, buckling, and spallation intensified surface degradation, and to uncontrolled destruction of the body of metallic component. The micro-mechanics of oxide layer delamination, buckling, and finally spallation were reviewed in References 8 and 21. A critical strain responsible for surface degradation by spallation was specified for instantaneous thickness of oxide layer (X), thermo-physical properties, and environmental loading (thermal gradient and mechanical stress). Therefore, the rate of function of surface degradation by spallation of surface oxide layer Θ in Eq. [1] was presented as a function of instant oxide layer thickness $K_S f(X)$, or more simply as $K_S X$, where K_S is the spallation constant for a specific severity of environmental loading and X is a thickness of the oxide layer:

$$\Theta = K_S f(X) \approx K_S X. \qquad [4]$$

In many cases, spallation occurred with sporadic frequency and was not uniformly localized through the surface. In our publication,[29] the spallation process was considered as a stochastic process with the frequency and sizes taken from the experimental measurement. In this article, the process of spallation was generalized as a function of instantaneous scale thickness X with spallation constant K_S governs a spallation intensity.

The oxide formed during high-temperature oxidation of metallic alloys typically have a negligibly small partial gas pressure and oxidized surfaces could be stable at normal and even low gaseous pressure atmospheres. However, some reactive gases, for example, water vapor, can modify formed oxides into other easy volatile species which will initiate vaporization of the oxide layer from metal surfaces. For example, austenitic stainless steels show good oxidation resistance in oxygen and air, because these steels form a protective Cr-rich $(Cr,Fe)_2O_3$ scale. In the presence of water vapor, the ability to withstand oxidation is diminished because *Cr*-oxide transforms into Cr-hydroxides.[10–12] Experimental measurements supported theoretical predictions of the effects of intrinsic (material properties) and extrinsic (temperature, pressure, velocity, atmosphere composition) factors on Cr vaporization rate.[10,12,24,30] For a specific severity of environmental loading, the rate of surface degradation by vaporization can be presented in Eq. [1] by the vaporization constant K_V. In some cases, the scale structure and composition could be modified during severe environmental loading, which will influence on the value of K_V value in Eq. [5]:

$$\Phi(\tau) = K_V \qquad [5]$$

Considering Eqs. [2] through [5], the resulting phenomenological Eq. [1] for high-temperature degradation of metallic surface in normal and extreme gaseous environment is shown in Eq. [6], where the rate of surface degradation (dX/dt) comprised of the parabolic rate of forming adherent oxide ($K_P/2X$), the vaporization rate (K_V), and the rate of scale spallation, which depends on instantaneous scale thickness X and spallation constant K_S:

$$dX/dt = K_P/2X - K_V - K_S X \qquad [6]$$

Equation [6] extends Eq. [7], which was suggested by Tedmon[25] and used in many publications.[24–30] Equation [7] treats all surface destruction processes, including spallation and/or vaporization, as a one time-dependent process with unified kinetic constant K_r:

$$dX/dt = K_P/2X - K_r \qquad [7]$$

The suggested phenomenological Eq. [1] of surface degradation of metallic materials was specified for a gaseous environment (Eq. [6]) and considers two types of surface destruction processes: the first type $\Phi(\tau)$ depends on a process time and the second type Θ depends on an instantaneous condition of a modified surface. Such representation provides a broader analysis of multiple phenomena involved in surface degradation of solid surface interacting with gaseous environments at normal and extreme loading conditions.

III. ANALYSIS OF GOVERNING EQUATION OF SURFACE DEGRADATION

Solving governing Eqs. [1] and [6] for determination of kinetic coefficients can be used for:

- lifetime prediction of metallic components for a known environmental severity,
- determination of a critical environmental severity for desired metallic component lifetime,
- verification of assumptions used in phenomenological description of the surface degradation kinetics, and
- shed light on the micro-mechanisms of surface degradation.

Considering at least three possible mechanisms of surface degradation of metallic materials in severe gaseous environmental condition (oxidation with forming adherent oxide layer, spallation, and vaporization), the kinetic constants then can be determined by combining analysis of phenomenological Eqs. [1] and [6] with experimental data. At least two principally different experimental approaches could be used to determine the individual kinetics. The first one is based on experimental design of such environmental conditions which could minimize a number of mechanisms, after which the kinetic constants could be defined for each process assuming its independence. For example, high-temperature oxidation assisted by vaporization of Cr-oxide was analyzed by controlling the specimen weight in two atmospheres: one with air, when only oxidation was expected, and the second with water vapor, when oxidation was assisted by intensive vaporization of Cr-hydroxides takes place.[37] Based on the comparison of two tests, the oxidation and vaporization constants were determined, assuming independence of oxidation kinetics from vaporization and *vice versa*.

However, it is difficult to design such experiments to separate more than two possible mechanisms of surface degradation. In this article, a methodology of determining the reaction constants for multiple processes of surface degradation in individual experiments is discussed and illustrated for several cases. A mass balance (Eq. [8]) calculates changing weight of the metallic specimen with adherent layer (ΔW) when two surface degradation processes take place, including time-proportional vaporization and integrated weight of spalled oxide linked to the instantaneous thickness of adherent oxide (X). A mass balance (Eq. [8]) includes two kinetic coefficients (K_V, cm/h and K_S, 1/h), metal oxide density (ρ_{ox}), and a weight fraction of oxygen-in oxide (f_O):

$$\Delta w = \rho_{ox} f_O X - \rho_{ox}(1 - f_O) K_V \tau - \rho_{ox}(1 - f_O) \int_0^\tau K_S X d\tau \qquad [8]$$

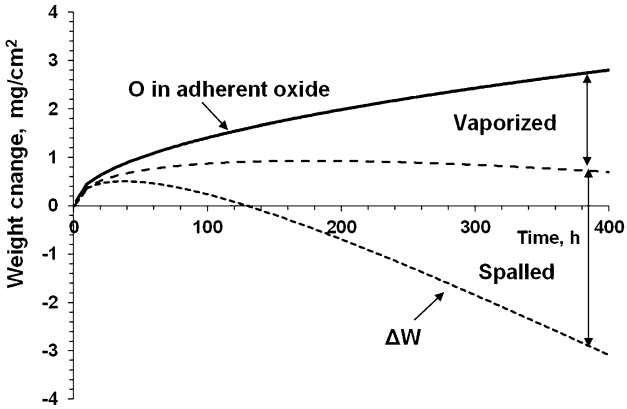

Fig. 2—Example of solving mass balance Eq. [8] for arbitrary values of kinetic constants K_P, K_V and K_S.

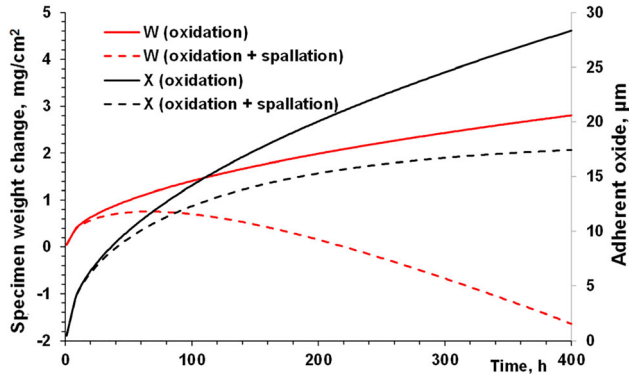

Fig. 3—Example of calculated adherent layer thickness and specimen mass changes for normal oxidation condition with forming adherent oxide $K_P = 2 \times 10^{-8}$ cm^2/h and during severe oxidation assisted by spallation with kinetic constant $K_S = 3 \times 10^{-3}$ 1/h at the same oxidation constant.

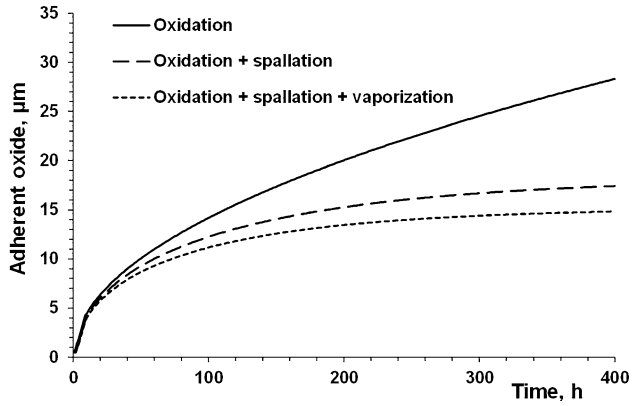

Fig. 4—Example of calculated adherent layer thickness for oxidation ($K_P = 2 \times 10^{-8}$ cm^2/h) assisted by spallation ($K_S = 3 \times 10^{-3}$ 1/h) and vaporization ($K_V = 2 \times 10^{-6}$ cm/h).

The term $\rho_{ox}(1 - f_O)K_V\tau$ describes the change of specimen weight due to vaporization. The actual process includes several steps: oxidation with increasing weight of the amount of oxygen, possible oxide to hydroxide modification in the presence of water vapor and followed by vaporization of the entire species. Because the sum of oxygen-in is equal to the sum of oxygen-out, the vaporization term in the mass balance includes just a specimen loss. This explains the multiplier $(1 - f_O)$. Integration with spallation constant K_S summarized instantaneous weight loss due to spallation in Eq. [8]. The solution of the differential Eq. [6], under assumption $X(0) = 0$, which links process time (τ, h) to the thickness of the oxidized adherent layer (X, cm) for the given set of kinetic coefficients for oxidation K_P (cm^2/h), for vaporization K_V (cm/h), and for spallation K_S (1/h) presents in Appendix (Eq. [A1]).

A Microsoft Excel numerical integrator was used to simulate all weight components in Eq. [8] and adherent oxide thickness X at process time τ. Figure 2 illustrates a mass balance during surface degradation at extreme environmental conditions, when formation of adherent oxide layer with kinetic constant $K_P = 2 \times 10^{-8}$ cm^2/h was assisted by metal vaporization with constant $K_V = 2 \times 10^{-6}$ cm/h, and spallation frequency with constant $K_S = 3 \times 10^{-3}$ 1/h. The range of these values was taken from our experimental study of oxidation of austenitic Cr/Ni heat-resistant steels.[33,34] A parabolic oxide growth, predicted for each oxidation time with a rate related to instantaneous thickness X, decreased due to spallation and vaporization. The resulting curve for specimen weight change (ΔW) had a maximum, which declined due to metal losses with spallation and vaporization, and each of these processes followed a general law formulated in Eqs. [1] and [6].

Figure 3 illustrates calculated weight changes of a specimen with adherent layer (ΔW) and adherent oxide layer thickness (X) for normal environmental oxidation and for severe environmental conditions with spallation $K_S = 3 \times 10^{-3}$ 1/h at the same oxidation constant $K_P = 2 \times 10^{-8}$ cm^2/h. The thickness of the adherent layer decreased by spallation reached a limit when the rate of oxidation was compensated by the rate of spallation and resulted in a weight change curve which has a maximum (ΔW_m) at time (τ_m).

The trend of the adherent layer becomes more complicated when all three surface degradation processes are involved. Figure 4. illustrates a calculated thickness of adherent layer for the same oxidation constant $K_P = 2 \times 10^{-8}$ cm^2/h, as a parabolically rising to infinity curve for only oxidation, stabilized by additional spallation ($K_S = 2 \times 10^{-3}$ 1/h) and decreased by vaporization with $K_V = 1 \times 10^{-6}$ cm/h.

IV. DETERMINATION OF KINETIC COEFFICIENTS OF SURFACE DEGRADATION

The provided simulation examples illustrate the existence of several characteristic points on the weight change curve which could help with the determination of kinetic constants when it is not possible to experimentally determine the individual surface degradation processes. Experimental thermogravimetric analysis (TGA) with monitoring only specimen weight is often used

Table II. Strategy to Define Oxidation, Vaporization, and Spallation Constant from One Experiment

Surface Degradation Process	Determined Constant	Experimental Routes	
		Direct	Indirect
Oxidation + Spallation + Vaporization	K_P K_V K_S	#1: $\Delta W = f(\tau)$, W_i^s, X_f #2: ΔW_i, W_i^s, X_f	ΔW_m,, ΔW_f, X_f

because it is difficult to collect the weight of spalled and vaporized materials at high gas flow velocity or during thermal cycling. However, in the case when the final amount of vaporized species is determined by condensing vapor, the vaporization constant K_p can be directly determined from this measurement.

The relationships followed from Eq. [6] at the characteristic points can be used to determine the kinetic constant with no need to continuously monitor all reaction products. When solid reaction product is determined only at the test end (τ_f), including the weight of specimen with adherent oxide (ΔW_f), the weight of spalled oxide (ΔW_f^s), and the final thickness of adherent scale (X_f), the vaporization constant (K_V) could be calculated from a final mass balance using Eq. [A2] in Appendix. The real metal oxide density (ρ_{ox}) and the weight fraction of oxygen-in oxide (f_O) in the adherent layer are to be experimentally verified because of the complexity of the layered oxide structure and internal defects. In our works,[29,34] determination of oxygen-in oxide (f_O) was done with combustion analysis of spalled oxides and the density of adherent oxidized layer (ρ_{ox}) from correlation between several measured layer thicknesses and specimen weight gains, when tests were done under the condition of no spallation.

When all three mechanisms were involved, we have $K_V > 0$, $K_S > 0$ and for any intermediate experimental time (τ_i), instant thickness X_i of adherent layer can be analytically calculated for a known weight of specimen (ΔW_i) and a weight of spalled (W_i^s) scale using Eq. [A3] in Appendix. Therefore, for series of observations of τ_i, ΔW_i , and W_i^s, a series of calculated values X_i can be determined from Eq. [A3] and this series may be used to calculate the constant K_S.

When only specimen weight was monitored in experiments, the characteristic point of a maximal weight of specimen with adherent layer (Figure 2; Eq. [3]) can be used for indirect analysis of two mechanisms using the relationships followed from Eq. [7]. This equation is valid for two mechanisms of surface degradation: one for parabolic oxidation and the other assumed to be proportional to process time, which could be vaporization of spallation.[25] For the three processes described in Eq. [6], the thickness of adherent layer (X_m) at a time (τ_m) when weight change of specimen with adherent layer achieved maximum (ΔW_m) was found using Eq. [A4] in Appendix. Unfortunately, it is difficult to measure the thickness of adherent layer X_m at a maximum point of weight gain ΔW_m; however, it is possible to approximate X_m using Eq. [A3] in Appendix. Table II presents the possible experimental routes to determine three kinetic constants.

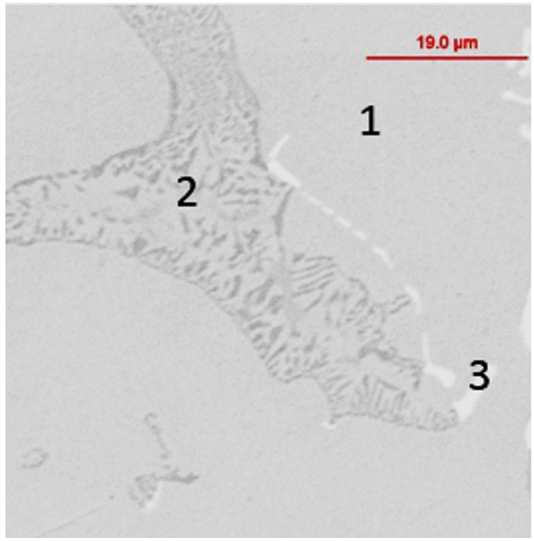

Fig. 5—SEM observed microstructure of studied steel: 1—austenite, 2—Cr–Fe complex carbides, and 3—Nb-carbonitrides.

V. KINETIC CONSTANTS FOR SURFACE DEGRADATION OF AUSTENITIC CR/NI STEEL IN SEVERE ENVIRONMENTAL CONDITIONS

A. *Experimental Procedures*

A laboratory cast Nb-bearing heat-resistant austenitic steel with 20Cr, 11Ni, 1.8Mn, 1.6Si, 0.41C, 1.7Nb, and 0.1N (in weight pct) was oxidized at 950 °C in two environmental conditions: test #1 was designed for oxidation assisted by spallation in air and test #2 for oxidation assisted by spallation and vaporization in water vapor combustion atmosphere (15 CO_2, 2 O_2, 15 water vapor, N_2—balance, vol pct) to initiate Cr-hydroxide volatilization. The used environmental conditions were verified in our previous studies.[29,34] The tests included static oxidation with periodic monitoring weight change of a specimen with adherent scale (ΔW, mg/cm^2) and a weight of spalled scale (W_s, mg/cm^2) during 400 hours test duration. Ten SEM measurements of the final adherent oxide thickness in cross section were done for specimens coated by epoxy. The mass portion of oxygen (f_o = 0.33) in the spalled scale was evaluated using the LECO N/O analyzer of the spalled scale. The SEM/EDX analysis of as-cast microstructure showed Nb-carbonitrides (white phase, point #3) and Cr–Fe carbides (gray phase, point #2) at the boundaries of primary austenite dendrites (matrix, phase #1) in Figure 5.

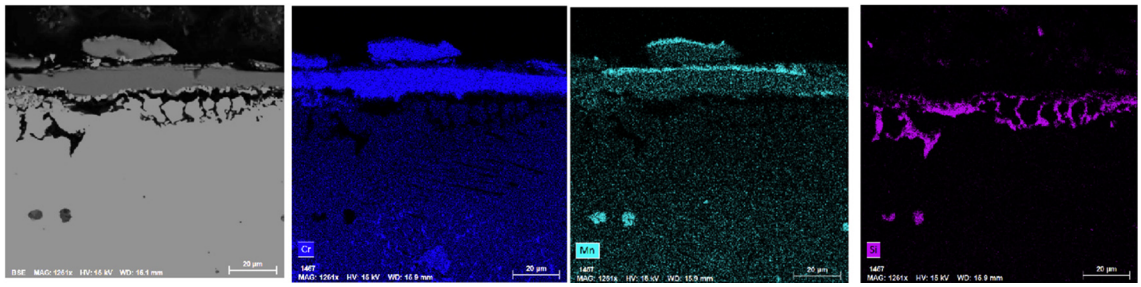

Fig. 6—Structure and chemical mapping of adherent oxide layer formed in studied austenitic steel in test #1 (950 °C, air, 400 h).

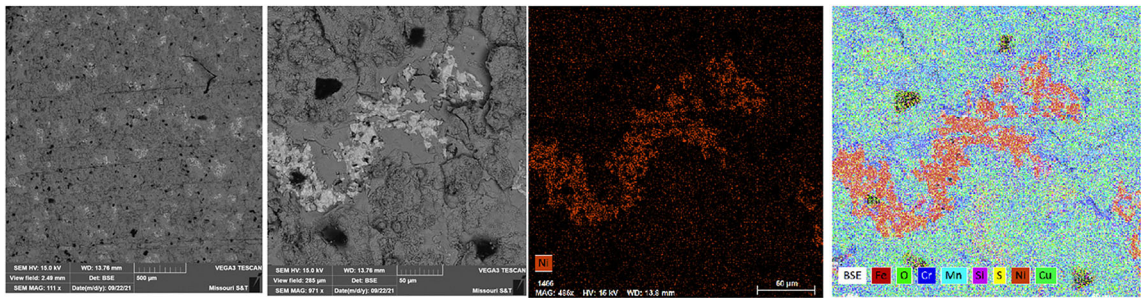

Fig. 7—Top view and chemical mapping of oxidized surface of studied austenitic steel in test #1 (950 °C, air, 400 h).

B. *Results*

After 400 hours duration in test #1, the multilayered scale structure in cross section had the averaged thickness within 12 ± 5 μm and consisted of external Fe–Mn oxides and internal Cr–Fe oxide mixture strongly adherent to Si-oxides sublayer (Figure 6). Repeated layer composition indicated old and newly developed oxide layers after partial spallation.

Therefore, when cracking and spallation occurs at the boundary between these layers, the spalled scale topology can be defined from experimental observation of the oxidized surface top view using an elemental surface map (Figure 7) and statistic of diameter of spalled spaces was used in stochastic simulations as was described in References 29 and 34.

The experimentally measured weight change of the specimen with an adherent layer (ΔW) and the spalled scale weight (W_s) are shown by markers in Figure 8(a). Because of intensive spallation, the specimen weight decreased after a maximum and it had a negative final value at 400 hours (ΔW_f). The spalled scale weight increased with test time. The total measured weight change from the specimen with the adherent layer and the spalled scale was positive. An experimentally determined fraction of oxygen-in oxide layer (f_o = 0.33) and the final thickness of adherent oxide (X_f = 12 μm) were used together with the recorded weights to calculate the oxidation, spallation, and vaporization kinetics. The developed integrator with built-in solver in Microsoft Excel was used to minimize an error between measured and simulated data (objective) by varying the kinetic constants and the targeted experimental value of the final adherent oxide thickness (X_f). The collected data (X_f, ΔW_f and W^s_f) at the experiment end (τ_f) indicated minor vaporization (Eq. [A2] in Appendix). The three optimized kinetic constants were defined: oxidation (K_P = 8.1 × 10^{-9} cm^2/h), vaporization K_V = 3 × 10 7 cm/h), and spallation (K_S = 2.1 × 10^{-3} 1/h). Calculated curves for model (Eq. [6]) were well fit with the experimental results, indicating two main surface degradation processes: oxidation and spallation (Figure 8(b)).

Test #2 was performed at the same 950 °C, but the synthetic water vapor atmosphere, to mimic gasoline engine combustion gas, was used instead of air. The observed final thickness of the adherent layer was 30 ± 10 μm. The specimen weight loss and the amount of spalled scale were about twice as large in test #2 when compared to test #1 at the same time/temperature test schedule. Combustion atmosphere in test #2 intensified oxidation and initiated vaporization of modified *Cr*-oxide to *Cr*-hydroxide. Figure 9(a) illustrates the recorded weights and simulated curves at the determined values of kinetic constants: oxidation (K_P = 5.7 × 10^{-8} cm^2/h), vaporization (K_V = 2.6 × 10^{-6} cm/h), and spallation (K_S = 1.9 × 10^{-3} 1/h). The calculated specimen weight had a maximum value at 70 hours test time and then dropped due to joint effect of spallation and vaporization. Figure 9(b) illustrates calculated surface degradation processes and experimental point for the measured thickness of the adherent oxide layer.

In this study, the oxidation, vaporization, and spallation kinetics were determined by using experimental measurements of at least three parameters (specimen weight change, weight of spalled scale, and final scale thickness). Figure 10 compares the intensity of different mechanisms of surface degradation for two studied cases. These tests were performed at the same temperature and time duration but in different atmospheric

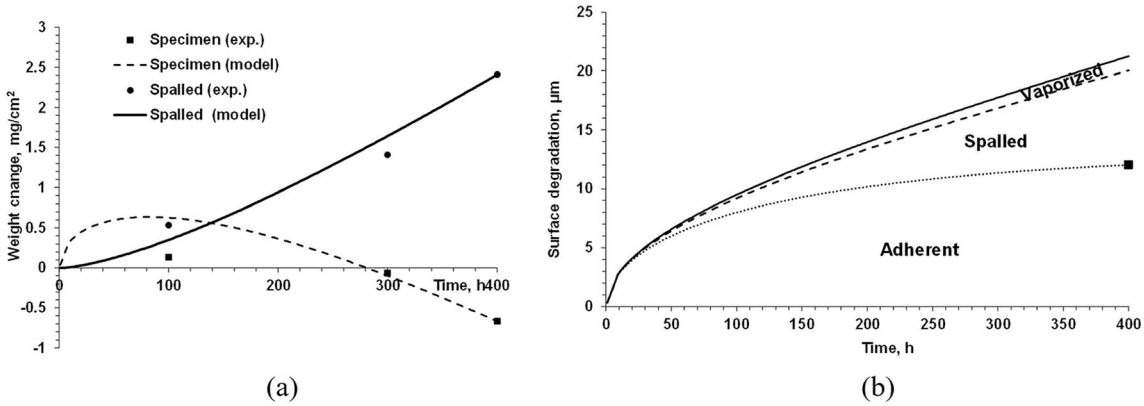

Fig. 8—Test #1 (950 °C, air): (*a*) experimentally measured and simulated weight change of specimen with adherent oxide and spalled scale and (*b*) recalculated surface degradation kinetics (experimental data are shown by markers).

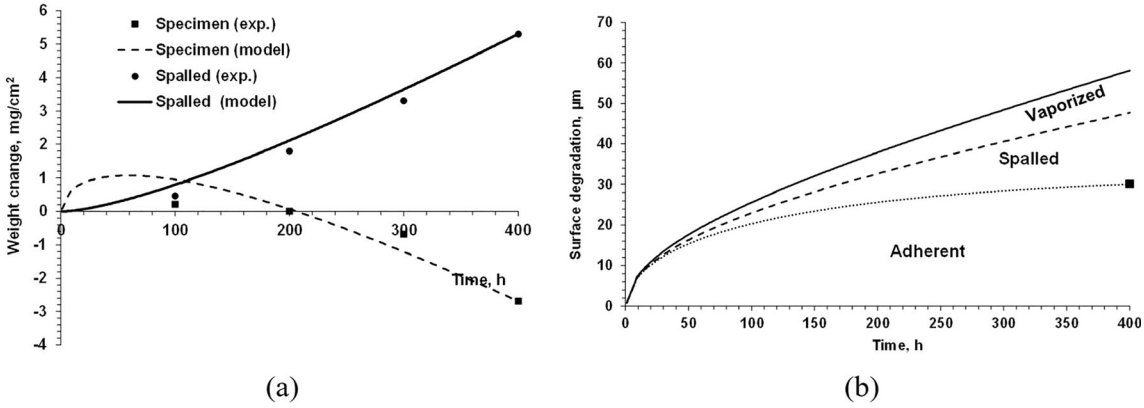

Fig. 9—Experimentally measured and simulated weight change of specimen with adherent oxide layer and weight of spalled scale (*a*) and calculated mechanisms of surface degradation with experimental points at the test end (*b*).

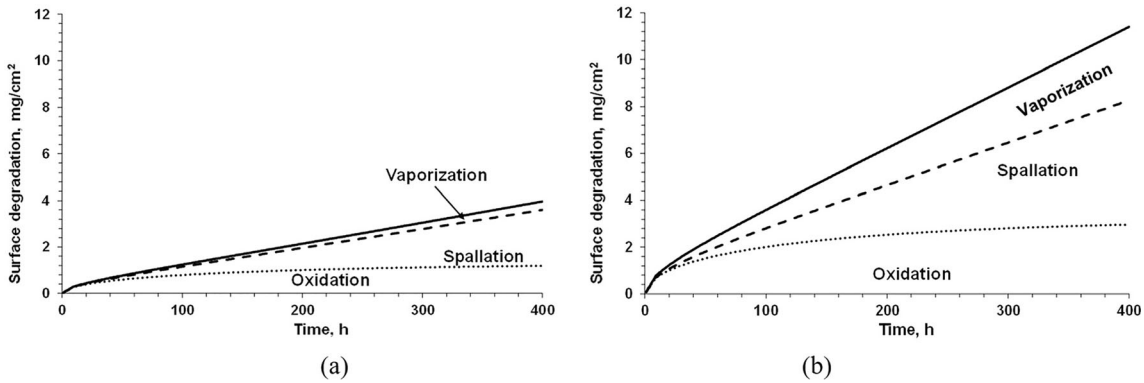

Fig. 10—Comparison of intensity of surface degradation mechanisms for different severity of environmental load: (*a*) test #1 in air and (*b*) test #2 in combustion atmosphere.

conditions. All three surface degradation mechanisms were accelerated in the presence of water vapor.

The developed integrator has options to include more parameters if deviations of spallation from oxide layer thickness or vaporization from time were determined in experiments. For example, a minimal scale thickness needed to initiate spallation was determined in tests,[29,33] which could be included in the integrator. Finally, the intensity of involved mechanisms of surface degradation of heat-resistant Cr/Ni austenitic steel controlled by a severity of environmental loading is schematically illustrated in Figure 11.

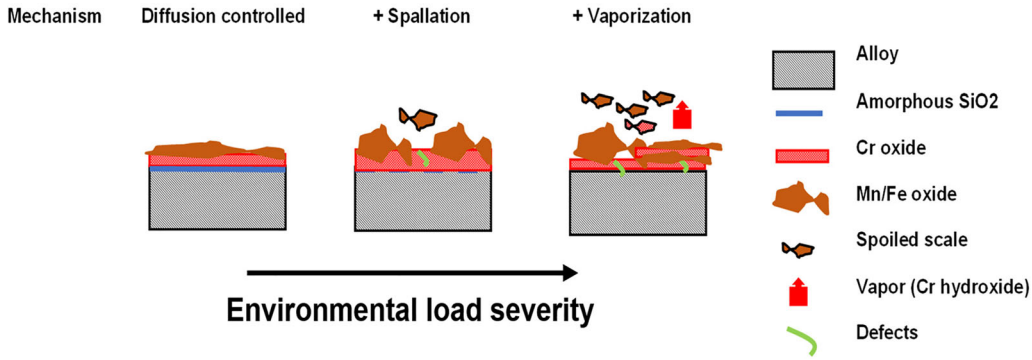

Fig. 11—Effect of environmental load severity from normal to extreme (temperature, atmosphere, mechanical stress) on surface degradation processes in Cr–Ni heat-resistant steels.

VI. CONCLUSIONS

The surface degradation of metallic materials in high-temperature aggressive gaseous atmosphere could be a joint result of several mechanisms:

- forming multiphase oxide layer adherent to the surface,
- partial spallation of formed oxide layer, and
- possible vaporization of formed compounds.

The governing equation, which describes these processes, including a parabolic growth of adherent layer, time-dependent vaporization, and cross-linked to instantaneous thickness of adherent layer spallation, was suggested. Several analytical relationships were found by solving the governing equation. For practical applications, the integrator with solver was used to optimize the values of three kinetic constants: oxidation, vaporization, and spallation.

The strategy to define oxidation, vaporization, and spallation constants from one experiment was suggested and illustrated for two cases of surface degradation of *Cr/Ni* heat-resistant steel during severe environmental conditions: first with oxidation assisted by spallation and the second when vaporization also occurred in water vapor environment.

The suggested methodology could be considered in future for the analysis of different types of surface degradation of solid materials in gaseous, liquid, or solid environments with time-dependent and cross-linked kinetics.

ACKNOWLEDGMENTS

Authors appreciate the support provided by Ford Motor and Missouri University of Science and Technology

CONFLICT OF INTEREST

On behalf of all authors, the corresponding author states that there is no conflict of interest.

APPENDIX

A1 The solution of the differential Eq. [6], under assumption $X(0) = 0$, links process time (τ, h) to the thickness of the oxidized adherent layer (X, cm) for the given set of kinetic coefficients for oxidation K_P (cm^2/h), for vaporization K_V (cm/h), and for spallation K_S (1/h):

$$\tau = \frac{K_V - G}{2K_S G} ln\left(\frac{2K_S X + K_V - G}{K_V - G}\right) - \frac{K_V + G}{2K_S G} ln\left(\frac{2K_S X + K_V + G}{K_V + G}\right) \quad [A1]$$

where: $G = \sqrt{K_V^2 + 2K_S K_p}$

A2 When solid reaction product is determined at the test end (τ_f), including the weight of specimen with adherent oxide (ΔW_f), the weight of spalled oxide (ΔW_f^s), and the final thickness of adherent scale (X_f), the vaporization constant (K_V) could be calculated from a final mass balance, assuming that the metal oxide density (ρ_{ox}), and the weight fraction of oxygen-in oxide (f_O) are known:

$$K_V = \frac{f_o X_f}{(1 - f_o)\tau_f} - \frac{\Delta W_f^s}{\rho_{ox}\tau_f} - \frac{\Delta W_f}{\rho_{ox}\tau_f(1 - f_o)} \quad [A2]$$

A3 When all three mechanisms were involved, we have $K_V > 0$, $K_S > 0$ and for any intermediate experimental time (τ_i), instant thickness X_i of adherent layer can be analytically calculated for a known weight of specimen (ΔW_i) and a weight of spalled (W_i^s) scale:

$$X_i = \frac{\Delta W_i}{\rho_{ox} f_o} + \frac{K_V(1 - f_o)\tau_i}{f_o} + \frac{W_i^s(1 - f_o)}{\rho_{ox} f_o} \quad [A3]$$

A4 When only specimen weight was monitored in experiments, the characteristic point of a maximal weight of specimen with adherent layer can be used for indirect analysis of surface degradation mechanisms. For the three processes described in Eq. [6], the thickness of adherent layer (X_m) at a time (τ_m) when weight change of specimen with adherent layer achieved maximum (ΔW_m) can be found:

$$\tau_m = \frac{K_V - G}{2K_S G}\ln\left(\frac{G_f - G}{K_V - G}\right) - \frac{K_V + G}{2K_S G}\ln\left(\frac{G_f + G}{K_V + G}\right)$$
$$X_m = \frac{G_f - K_V}{2K_S} \qquad [A4]$$

where $G = \sqrt{K_V^2 + 2K_S K_p}$ and $G_f = \sqrt{K_V^2 + 2K_S K_p f_O}$.

REFERENCES

1. R. Jojith, M. Sam, and N. Radhika: *Eng. Sci. Technol. Int. J.*, 2022, vol. 25, pp. 1–7.
2. A. Khan, A. Qurashi, W. Badeghaish, M. Noui-Mehidi, and M. Aziz: *Sensors (Basel)*, 2020, vol. 20, p. 6583.
3. E. Stansbury and R. Buchanan: *Fundamentals of Electrochemical Corrosion*, ASM International, Materials Park, 2020.
4. G. Xu, K. Wang, X. Dong, L. Yang, M. Ebrahimi, H. Jiang, Q. Wang, and W. Ding: *J. Mater. Sci. Technol. Technol.*, 2021, vol. 71, pp. 12–22.
5. L. Ma, C. Zhang, Y. Wu, and I. Yuanwei: *Sol. Energy Mater. Sol. Cell*, 2022, vol. 234, p. 111485.
6. R. Chen and W. Yeun: *Oxid. Met.*, 2003, vol. 59, pp. 433–68.
7. C. Taylor and B. Tossey: *Mater. Degrad.*, 2021, vol. 5, p. 38.
8. H.E. Evans: *Int. Mater. Rev.*, 1995, vol. 40, pp. 1–40.
9. R. Pillai, A. Chyrkin, and W. Quadakkers: *Oxid. Met.*, 2021, vol. 96, pp. 385–436.
10. H. Asteman, J. Svensson, and L. Johansson: *J. Electrochem. Soc.*, 2004, vol. 15, p. B141.
11. M. Romedenne, R. Pillai, S. Dryepondt, and B. Pint: *Oxid. Met.*, 2021, vol. 96, pp. 589–612.
12. D. Young and B. Pint: *Oxid. Met.*, 2006, vol. 66, pp. 137–53.
13. C. Taylor: *Corros. Eng. Sci. Technol.*, 2015, vol. 50, pp. 490–508.
14. S. Bigdeli, L. Kjellqvist, R. Naraghi, L. Hoglund, H. Larsson, and T. Jonsson: *J. Phase Equilib. Diffus.*, 2021, vol. 42, pp. 403–18.
15. W. Blades, E. Opila, and K. Sieradzki: *J. Electrochem. Soc.*, 2022, vol. 169, p. 061501.
16. H. Mehrer and G. Murch: *Diffus. Found.*, 2021, vol. 29, pp. 1–30.
17. R. Osei, S. Lekakh, and R. O'Malley: *Metall. Mater. Trans. B*, 2021, vol. 52B, pp. 393–404.
18. J. Philibert: *Solid State Ion.*, 1999, vol. 117, pp. 1–7.
19. O. Kubaschewski and B.E. Hopkins: *Oxidation of Metals and Alloys*, Butterworths, London, 1962.
20. V. Rosenband, A. Gany, and Y. Timnat: *Oxid. Met.*, 1995, vol. 43, pp. 141–56.
21. H. Evans, G. Mitchell, R. Lobb, and D. Owen: *Proc. R. Soc. Lon. A*, 1993, vol. 440, pp. 1–22.
22. R. Pillai, M. Romedenne, J. Peng, B. Pint, J.J. Haynes, G. Muralidharan, and D. Shin: *Oxid. Met.*, 2022, vol. 97, pp. 51–76.
23. R. Auguste, R. Chan, and E. Romanovskaia: *Mater. Degrad.*, 2022, vol. 6, p. 61.
24. T. Sand, C. Geers, Y. Cao, J. Svensson, and L. Johansson: *Oxid. Met.*, 2019, vol. 92, pp. 259–79.
25. C. Tedmon: *J. Electrochem. Soc.*, 1966, vol. 113, pp. 766–69.
26. C. Lowell, C. Barrett, R. Palmer, J. Auping, and H. Probst: *Oxid. Met.*, 1991, vol. 36, pp. 81–112.
27. R. Duan, A. Jalowicka, K. Unocic, B. Pint, P. Huczkowski, A. Chyrkin, D. Grüner, R. Pillai, and W. Quadakkers: *Oxid. Met.*, 2017, vol. 87, pp. 11–38.
28. D. Poquillon and D. Monceau: *Oxid. Met.*, 2003, vol. 59, pp. 409–31.
29. S. Lekakh, O. Neroslavsky, M. Li, and L. Godlevski: *Oxid. Met.*, 2022, vol. 98, pp. 239–54.
30. B. Pujilaksono, T. Jonsson, M. Halvarsson, I. Panas, J. Svensson, and L. Johansson: *Oxid. Met.*, 2008, vol. 70, pp. 163–88.
31. J. Smialek: *High Temp. Corros. Mater.*, 2023, vol. 99, pp. 431–57.
32. S. Sureau, D. Poquillon, and D. Monceau: *Scr. Mater.*, 2007, vol. 56, pp. 233–36.
33. S. Lekakh, O. Neroslavsky, M. Li, and L. Godlevski: *High Temp. Corros. Mater.*, 2023, vol. 99, pp. 79–99.
34. S. Lekakh, M. Buchely, M. Li, and L. Godlevski: *Mater. Sci. Eng. A*, 2023, vol. 873, p. 145027.
35. R. Rapp: *Metall. Trans. A*, 1984, vol. 15A, pp. 765–82.
3A6. Y. Chen, T. Tan, and H. Chen: *J. Nucl. Sci. Technol.*, 2008, vol. 45, pp. 662–67.
37. N. Jacobson, M. Kuczmarski, and B. Kowalski: *Oxid. Met.*, 2020, vol. 93, pp. 247–82.

Publisher's Note Springer Nature remains neutral with regard to jurisdictional claims in published maps and institutional affiliations.

Springer Nature or its licensor (e.g. a society or other partner) holds exclusive rights to this article under a publishing agreement with the author(s) or other rightsholder(s); author self-archiving of the accepted manuscript version of this article is solely governed by the terms of such publishing agreement and applicable law.